

# Constraining Axion and ALP Dark Matter from Misalignment during Reheating

---

**Yong Xu**

*PRISMA<sup>+</sup> Cluster of Excellence and Mainz Institute for Theoretical Physics, Johannes Gutenberg University, 55099 Mainz, Germany*

*E-mail:* [yonxu@uni-mainz.de](mailto:yonxu@uni-mainz.de)

**ABSTRACT:** We explore the phenomenology of QCD axion and axion-like particle (ALP) dark matter production via misalignment during inflationary reheating. We investigate scenarios involving inflaton oscillating in a generic potential  $\sim \phi^n$ , considering inflaton decay and annihilation for reheating. For low reheating temperatures, the parameter space leading to the correct relic abundance can be enlarged beyond the standard case. Depending on the type of inflaton-matter couplings and the value of  $n$ , we find that certain parts of the extended parameter space are already constrained by ADMX, CAPP, and MUSE experiments. Future Haloscope experiments are expected to impose more stringent constraints. We highlight the potential to utilize axion experiments in constraining the dynamics of reheating.

---

## Contents

<b>1</b>	<b>Introduction</b>	<b>1</b>
<b>2</b>	<b>Reheating</b>	<b>3</b>
<b>3</b>	<b>Misalignment after Reheating: <math>T_{\text{rh}} \geq T_{\text{osc}}</math></b>	<b>5</b>
3.1	QCD Axion	5
3.2	ALP	7
<b>4</b>	<b>Misalignment during Reheating: <math>T_{\text{rh}} &lt; T_{\text{osc}}</math></b>	<b>7</b>
4.1	QCD Axion	8
4.1.1	Case 1: $T_{\text{QCD}} < T_{\text{osc}}$	8
4.1.2	Case 2: $T_{\text{QCD}} \geq T_{\text{osc}}$	10
4.2	ALP	13
<b>5</b>	<b>Experimental Constraints</b>	<b>14</b>
5.1	Results	15
5.2	Probing Reheating via Axion Experiments	18
<b>6</b>	<b>Conclusions</b>	<b>19</b>

---

## 1 Introduction

QCD axions and axion-like particles (ALPs) are among the well motivated candidates for cold dark matter (DM) [1–4]. They are pseudo-Nambu-Goldstone bosons, arising from the spontaneous breaking of some global  $U(1)$  symmetry [5–8] or low energy effective field theory emerging from string theory [9–13]. See Refs. [14, 15] for reviews on the recent progress on axions and ALPs. In the early universe, cold axion and ALP DM can be copiously sourced<sup>1</sup> via the vacuum misalignment mechanism [22–24].

In the standard scenario where oscillations begin during the radiation-dominated epoch, the relic abundance of QCD axions depends on both the mass  $m_a$  and the initial misalignment angle  $\theta_i$ . For  $\theta_i \sim \mathcal{O}(1)$ <sup>2</sup>, a mass window in the range  $(10^{-6} \text{ eV}, 10^{-5} \text{ eV})$  is necessary to match observed DM relics. For ALPs, besides the mass and initial misalignment angle, the relic abundance is also dependent on the decay constant. Similarly, the parameter space is limited unless the initial misalignment angle is not  $\mathcal{O}(1)$ . In literature,

---

<sup>1</sup>Alternatively, scatterings in the thermal plasma and the decay of topological defects can also source axion [16]. Relativistic axions can be sourced via evaporation of primordial black holes [17–20]. In dense environments, such as red giants, white dwarfs or neutron stars, axions can be produced abundantly via the Bremsstrahlung processes [21].

<sup>2</sup>Assuming that  $\theta_i$  follows a uniform distribution from  $-\pi$  to  $\pi$ , the average is  $\sqrt{\langle \theta_i^2 \rangle} = \pi/\sqrt{3}$  [25].

it is demonstrated that for low-scale inflation, axions could follow a Bunch-Davies distribution, allowing for a smaller initial misalignment angle [26, 27], which in turn can widen the parameter space. Additionally, models with nonzero initial velocity, namely  $\dot{\theta}_i \neq 0$ , could also extend the axion window [28–30]. Here, we primarily focus on the simplest and most traditional scenario with  $\theta_i \sim \mathcal{O}(1)$  and assume  $\dot{\theta}_i = 0$  [25]. In this case, it has been shown that deviations from standard cosmological histories—such as the presence of early matter or kination epochs—can significantly broaden the parameter space for both axions and ALPs [17, 19, 31–43].

In this paper, we explore the generation of axion and ALP DM via misalignment mechanism during inflationary reheating.<sup>3</sup> Reheating affects the parameter space compatible with the observed relic abundance in two ways. First, the entropy injection during reheating is expected to enlarge the parameter space, possibly encompassing regions accessible to current and future Haloscope experiments [62, 63]. It is revealed that the degree of entropy injection is intricately linked to the dynamics of reheating, depending on factors such as the shape of the inflaton potential and the nature of inflaton-matter couplings [55, 64]. Moreover, when assuming misalignment during reheating, the oscillation temperature (another important factor determining the parameter space) is controlled by the underlying reheating scenarios. These connections underscore the correlation between the augmented parameter space and the underlying reheating dynamics.

Here, our aim is to determine the parameter space for axion and ALP DM resulting from misalignment during reheating, while also exploring the corresponding experimental constraints from Haloscope and Telescope experiments. The primary objective of this study is to investigate the impact of reheating dynamics, particularly the shape of the inflaton potential and the type of inflaton-matter couplings, on the parameter space. Furthermore, we aim to analyze the associated experimental constraints. Additionally, we explore the potential of utilizing axion experiments to constrain reheating scenarios. To achieve this, we focus on a scenario where the inflaton oscillates around a general potential proportional to  $\phi^n$  during reheating.<sup>4</sup> Additionally, we encompass a wide range of possibilities by considering reheating scenarios arising from both inflaton decays to scalars or fermions and annihilations to scalars.

Note that the current scenario is more general compared to what has been studied in the literature. To begin with, the two special cases<sup>5</sup> with  $n = 2$  and  $n \rightarrow \infty$  will recover the aforementioned scenarios where misalignment occurred during early matter and kination epochs. It is then expected that our scenario with  $n = 2$  and  $n \rightarrow \infty$  can reproduce the recent results in the literature, such as those in Ref. [42] and Ref. [40] for axions and ALPs misalignment during early matter and kination epochs. We will go beyond these two special cases; in particular, we will provide analytical expressions for any general  $n$ . Most importantly, we will also investigate the effect of inflaton-matter couplings on the

---

<sup>3</sup>This is complementary to recent investigations regarding DM production during reheating via other mechanisms, such as freeze-out or freeze-in [44–61].

<sup>4</sup>We assume that  $n$  is an even number to ensure the existence of a minimum.

<sup>5</sup>For a coherent scalar field oscillating around  $\sim \phi^n$ , the equation-of-state parameter is  $\omega = (n-2)/(n+2)$  [65]. Therefore,  $\omega = 0$  for  $n = 2$  and  $\omega = 1$  for  $n \rightarrow \infty$ .

axion and ALP DM parameter space, which has not been explored in the literature. This is particularly interesting since it offers a potential new avenue to probe reheating using axion experiments.

The rest of the paper is organized as follows. In Sec. 2, we revisit reheating with a particular focus on the evolution of energy densities and temperature. In Sec. 3, we briefly review misalignment in the radiation epoch after reheating. In Sec. 4, we investigate the phenomenology and parameter space for misalignment occurring during reheating. In Sec. 5, we present the experimental constraints and comment on how axion experiments can be used to constrain reheating. Finally, we summarize our findings in Sec. 6.

## 2 Reheating

After cosmic inflation ends, the inflaton starts to oscillate around the minimum of its potential, transferring energy to daughter particles that eventually thermalize and form a thermal bath [66–68]. Here, we assume that the inflaton potential during reheating takes the form  $\sim \phi^n$  with  $n$  being an even integer, which could originate from  $\alpha$  attractor inflation models [69], the Starobinsky inflation [70], or polynomial inflation models [71–73]. During reheating, the inflaton and radiation energy densities (denoted as  $\rho_\phi$  and  $\rho_R$ , respectively) can be tracked using the following Boltzmann equations [55, 64]:

$$\frac{d\rho_\phi}{dt} + \frac{6n}{n+2}H\rho_\phi = -\frac{2n}{n+2}\Gamma\rho_\phi; \quad (2.1)$$

$$\frac{d\rho_R}{dt} + 4H\rho_R = +\frac{2n}{n+2}\Gamma\rho_\phi, \quad (2.2)$$

where  $H = \sqrt{(\rho_\phi + \rho_R)/(3M_P^2)}$  corresponds to the Hubble parameter with  $M_P$  representing the reduced Planck mass, and  $\Gamma$  denotes the inflaton decay or annihilation rates into the radiation bath. In this work, we assume that the inflaton is a gauge singlet scalar field and consider inflaton decays into a pair of  $\varphi$  scalars (e.g., the Higgs field in the standard model) or vector-like fermions  $\psi$  (e.g., right-handed neutrinos) or annihilation into scalars. For bosonic and fermionic decays, they can proceed via trilinear interactions  $\sim \mu\phi|\varphi|^2$  and  $\sim y\phi\bar{\psi}\psi$ ; for bosonic annihilation, the interaction can be described by  $\sim \lambda\phi^2|\varphi|^2$ . With these interactions, we can then compute the inflaton energy transfer rates, which are given by:

$$\Gamma = \begin{cases} \frac{\mu_{\text{eff}}^2}{8\pi m_\phi} & \text{bosonic decay,} \\ \frac{y_{\text{eff}}^2 m_\phi}{8\pi} & \text{fermionic decay,} \\ \frac{\lambda_{\text{eff}}^2 \rho_\phi}{16\pi m_\phi^3} & \text{bosonic annihilation,} \end{cases} \quad (2.3)$$

where  $\mu_{\text{eff}}$ ,  $y_{\text{eff}}$  and  $\lambda_{\text{eff}}$  correspond to effective couplings after averaging over inflaton oscillations [64, 74], and  $m_\phi$  denotes the inflaton mass parameter, which is given by the second derivative of the potential  $\propto \phi^{n-2}$  [55, 64].

We define the end of reheating, or the onset of radiation epoch to be the moment when  $\rho_\phi(\mathbf{a}_{\text{rh}}) = \rho_R(\mathbf{a}_{\text{rh}}) = 3H(\mathbf{a}_{\text{rh}})^2 M_P^2$ , where  $\mathbf{a}_{\text{rh}}$  is the corresponding scale factor at that moment. In the regime with  $\Gamma \ll H$ , the solution for Eq. (2.1) during reheating can be approximated as [55, 64]

$$\rho_\phi(\mathbf{a}) \simeq \rho_\phi(\mathbf{a}_{\text{rh}}) \left( \frac{\mathbf{a}_{\text{rh}}}{\mathbf{a}} \right)^{\frac{6n}{2+n}}. \quad (2.4)$$

The Hubble parameter can then be expressed as follows:

$$H(\mathbf{a}) \simeq H(\mathbf{a}_{\text{rh}}) \begin{cases} \left( \frac{\mathbf{a}_{\text{rh}}}{\mathbf{a}} \right)^{\frac{3n}{n+2}} & \text{for } \mathbf{a}_{\text{end}} \leq \mathbf{a} \leq \mathbf{a}_{\text{rh}}, \\ \left( \frac{\mathbf{a}_{\text{rh}}}{\mathbf{a}} \right)^2 & \text{for } \mathbf{a}_{\text{rh}} \leq \mathbf{a}, \end{cases} \quad (2.5)$$

where  $\mathbf{a}_{\text{end}}$  denotes the scale factor at the end of inflaton. The first piece of Eq. (2.5) is obtained by using Friedmann equation with Eq. (2.4), and the second piece corresponds to the values during the radiation epoch. Using Eq. (2.3), Eq. (2.4) and Eq. (2.5), one can solve Eq. (2.2) and obtain the solution for  $\rho_R$  during reheating [55, 64]:

$$\rho_R(\mathbf{a}) \simeq \begin{cases} \frac{n}{1+2n} \rho_\phi(\mathbf{a}_{\text{rh}}) \left( \frac{\mathbf{a}_{\text{rh}}}{\mathbf{a}} \right)^{\frac{6}{n+2}} \left[ 1 - \left( \frac{\mathbf{a}_{\text{end}}}{\mathbf{a}} \right)^{\frac{2+4n}{2+n}} \right] & \text{bosonic decay,} \\ \frac{n}{7-n} \rho_\phi(\mathbf{a}_{\text{rh}}) \left( \frac{\mathbf{a}_{\text{rh}}}{\mathbf{a}} \right)^4 \left[ \left( \frac{\mathbf{a}_{\text{end}}}{\mathbf{a}} \right)^{\frac{2(n-7)}{2+n}} - 1 \right] & \text{fermionic decay,} \\ \frac{n}{2n-5} \rho_\phi(\mathbf{a}_{\text{rh}}) \left( \frac{\mathbf{a}_{\text{rh}}}{\mathbf{a}} \right)^{\frac{18}{n+2}} \left[ 1 - \left( \frac{\mathbf{a}_{\text{end}}}{\mathbf{a}} \right)^{\frac{2(2n-5)}{2+n}} \right] & \text{bosonic annihilation.} \end{cases} \quad (2.6)$$

From Eq. (2.6), we can further compute the thermal bath temperature  $T(\mathbf{a}) = [\rho_R(\mathbf{a}) 30/(\pi^2 g_\star)]^{1/4}$ , where  $g_\star$  denotes the degrees of freedom contributing the radiation energy densities. We find that the thermal bath temperature can be expressed as the following general expression [55, 64]:

$$T(\mathbf{a}) \simeq T_{\text{rh}} \begin{cases} \left( \frac{\mathbf{a}_{\text{rh}}}{\mathbf{a}} \right)^\alpha & \text{for } \mathbf{a}_{\text{end}} \leq \mathbf{a} \leq \mathbf{a}_{\text{rh}}, \\ \left( \frac{\mathbf{a}_{\text{rh}}}{\mathbf{a}} \right)^1 & \text{for } \mathbf{a}_{\text{rh}} \leq \mathbf{a}, \end{cases} \quad (2.7)$$

where the  $\alpha$  parameters are given by

$$\alpha = \begin{cases} \frac{3}{2(n+2)} & \text{bosonic decay,} \\ \frac{3(n-1)}{2(n+2)} & \text{fermionic decay,} \\ \frac{9}{2(n+2)} & \text{bosonic annihilation.} \end{cases} \quad (2.8)$$

We can then write the Hubble parameter in Eq. (2.5) as function of temperature:

$$H(T) \simeq \begin{cases} H(T_{\text{rh}}) \left( \frac{T}{T_{\text{rh}}} \right)^{\frac{3n}{2+n} \frac{1}{\alpha}} & \text{for } T_{\text{rh}} \leq T, \\ H(T_{\text{rh}}) \left( \frac{T}{T_{\text{rh}}} \right)^2 & \text{for } T \leq T_{\text{rh}}. \end{cases} \quad (2.9)$$

Several comments in order before closing this section. First, for bosonic annihilation with  $n = 2$ , it is not possible for the radiation to surpass inflaton energy densities as  $\rho_R \propto (\mathbf{a}_{\text{rh}}/\mathbf{a})^4$  while  $\rho_\phi \propto (\mathbf{a}_{\text{rh}}/\mathbf{a})^3$  during reheating. Therefore, we need to consider  $n > 2$  to achieve successful reheating and allow the universe to transition into a radiation-dominated epoch. Secondly, in the fermionic decay scenario with for  $n > 7$ , one has  $\alpha = 1$  because  $(\mathbf{a}_{\text{end}}/\mathbf{a})^{2(n-7)/(2+n)} \ll 1$  (in the second line of Eq. (2.6)). Furthermore, the analytical results, in particular Eq. (2.7) and Eq. (2.9), rely on the assumption that the dominant contribution for estimating temperature arises from perturbative inflaton decays. This assumption remains valid under the condition that the impact of non-perturbative phenomena [68, 75], and gravitational effects during reheating [76] remain subordinate to perturbative decay. It is important to note that even though the presence of non-perturbative processes could lead to the equation-of-state parameter  $\omega$  approaching  $1/3$ , perturbative decay retains its significance in fully depleting inflaton energy [77–79]. Moreover, for the bosonic decay scenario, investigations have highlighted the inefficacy of preheating due to the backreaction stemming from the self-interaction of the daughter field [77]. Similarly, fermionic preheating could be impeded by Pauli blocking [80]. These conclusions are expected to be more robust for weak couplings between the inflaton and daughter particles, a regime that aligns with low reheating temperatures. Finally, the gravitational reheating mechanism demands  $\omega = (n - 2)/(n + 2) \gtrsim 0.65$  to exert efficiency [57, 76, 81, 82], which effectively confines its significance to cases where  $n \lesssim 9$ .

In this study, we mainly focus on  $2 \leq n \leq 8$  with low reheating temperatures characterized by weak couplings, specifically  $T_{\text{rh}} \lesssim 1$  GeV. In these situations, it is reasonable to concentrate on perturbative processes and utilize the elementary theory of reheating based on perturbative decay [25].

### 3 Misalignment after Reheating: $T_{\text{rh}} \geq T_{\text{osc}}$

In this section we revisit the standard case where axion and ALP misalignment occurs during radiation epoch *after* reheating.

#### 3.1 QCD Axion

The axion mass  $m_a$  at zero temperature is given by [83]

$$m_a \simeq 5.7 \cdot 10^{-6} \left( \frac{10^{12} \text{ GeV}}{f_a} \right) \text{ eV}, \quad (3.1)$$

where  $f_a$  denotes the decay constant. The temperature-dependent axion mass  $\tilde{m}_a$  was numerically calculated in Ref. [84], which can be analytically approximated as [42, 43]

$$\tilde{m}_a(T) \simeq m_a \begin{cases} (T_{\text{QCD}}/T)^4 & \text{for } T \geq T_{\text{QCD}}, \\ 1 & \text{for } T \leq T_{\text{QCD}}, \end{cases} \quad (3.2)$$

where  $T_{\text{QCD}} \simeq 150$  MeV.

The Lagrangian density for axion field is

$$\mathcal{L}_a \supset \frac{1}{2} \partial^\mu a \partial_\nu a - \tilde{m}_a^2(T) f_a^2 \left[ 1 - \left( \cos \frac{a}{f_a} \right) \right], \quad (3.3)$$

with which one can derive the equation of motion of the axion field:

$$\ddot{\theta} + 3H \dot{\theta} + \tilde{m}_a^2(T) \sin \theta = 0, \quad (3.4)$$

where  $H$  denotes the Hubble expansion rate and  $\theta \equiv a(t)/f_a$ . At high temperature with  $T \gg T_{\text{QCD}}$ , the Hubble parameter is much larger than the axion mass so that the axion field is frozen to be constant. Axions begin to oscillate at the temperature  $T = T_{\text{osc}}$  defined by  $3H(T_{\text{osc}}) \equiv \tilde{m}_a(T_{\text{osc}})$  [25]. In the radiation epoch, the corresponding oscillation temperature is

$$T_{\text{osc}} \simeq \begin{cases} \left( \frac{1}{\pi} \sqrt{\frac{10}{g_\star}} m_a M_P \right)^{1/2} & T_{\text{osc}} \leq T_{\text{QCD}}, \\ \left( \frac{1}{\pi} \sqrt{\frac{10}{g_\star}} m_a M_P T_{\text{QCD}}^4 \right)^{1/6} & T_{\text{osc}} \geq T_{\text{QCD}}, \end{cases} \quad (3.5)$$

where we have used the second line of Eq. (2.9) for the Hubble parameter. Under the assumption that the entropy is conserved after reheating, we can relate the axion energy density at present with that at oscillation:

$$\rho_a(T_0) = \rho_a(T_{\text{osc}}) \frac{m_a}{\tilde{m}_a(T_{\text{osc}})} \frac{s(T_0)}{s(T_{\text{osc}})}, \quad (3.6)$$

where  $T_0 \simeq 2.73 \text{ K}$  denotes the temperature at present, and  $\rho_a(T_{\text{osc}}) \simeq \frac{1}{2} \tilde{m}_a^2(T_{\text{osc}}) f_a^2 \theta_i^2$  with  $\theta_i$  being the initial misalignment angle. The entropy density is defined as

$$s(T) = \frac{2\pi^2}{45} g_{\star s}(T) T^3, \quad (3.7)$$

where  $g_{\star s}$  denotes the degrees of freedom contributing to the SM entropy. Using Eq. (3.6) and Eq. (3.2), we can compute the axion relic abundance, which is

$$\Omega_a h^2 \equiv \frac{\rho_a(T_0)}{\rho_c/h^2} \simeq 0.12 \left( \frac{\theta_i}{1.0} \right)^2 \begin{cases} \left( \frac{m_a}{5.2 \cdot 10^{-7} \text{ eV}} \right)^{-\frac{3}{2}} & \text{for } m_a \leq m_a^{\text{QCD}}, \\ \left( \frac{m_a}{8.5 \cdot 10^{-6} \text{ eV}} \right)^{-\frac{7}{6}} & \text{for } m_a \geq m_a^{\text{QCD}}, \end{cases} \quad (3.8)$$

with  $\rho_c = 1.05 \cdot 10^{-5} h^2 \text{ GeV}^3/\text{cm}^3$  being the critical energy density,  $s(T_0) \simeq 2.69 \cdot 10^3 \text{ cm}^{-3}$  [85], and  $m_a^{\text{QCD}} \equiv m_a(T_{\text{osc}} = T_{\text{QCD}}) = 3H(T_{\text{QCD}}) \simeq 4.8 \cdot 10^{-11} \text{ eV}$ . By assuming an initial misalignment angle  $\theta_i \simeq 1.0$ , we see from Eq. (3.8) that a axion mass around  $m_a \sim \mathcal{O}(10^{-5}) \text{ eV}$ , and correspondingly a decay constant  $f_a \sim \mathcal{O}(10^{12}) \text{ GeV}$  is required in order to match the observed relic abundance.

### 3.2 ALP

For ALP, we remain model agnostic about the origin of its mass. We consider ALP mass to be time independent, and the oscillation temperature is then given by the first line of Eq. (3.5). The energy density at present takes a form:

$$\rho_a(T_0) = \rho_a(T_{\text{osc}}) \frac{s(T_0)}{s(T_{\text{osc}})}, \quad (3.9)$$

where  $\rho_a(T_{\text{osc}}) \simeq \frac{1}{2} f_a^2 m_a^2 \theta_i^2$ . Similar as before, we can further compute the relic abundance for ALPs, which is

$$\Omega_a h^2 \simeq 0.12 \left( \frac{\theta_i}{1.0} \right)^2 \left( \frac{f_a}{1.0 \cdot 10^{14} \text{ GeV}} \right)^2 \left( \frac{m_a}{7.4 \cdot 10^{-11} \text{ eV}} \right)^{1/2}. \quad (3.10)$$

Note that in general  $f_a$  and  $m_a$  are independent parameters for ALP, however it is required that  $f_a \propto m_a^{-1/4}$  in order to match the observed DM relic abundance. Besides, as a way of cross checking, we notice that once replacing  $f_a$  to be  $m_a$  via Eq. (3.1), Eq. (3.10) reproduces the first line of Eq. (3.8).

In the next section, we will explore the phenomenological consequence of misalignment occurring *during* reheating. Depending on the dynamics of reheating, we will show that both the axion and ALP DM parameter space can be enlarged and show distinct behaviours.

### 4 Misalignment during Reheating: $T_{\text{rh}} < T_{\text{osc}}$

In the previous section we have assumed that the oscillation temperature is  $T_{\text{osc}} < T_{\text{rh}}$  so that misalignment occurs in radiation epoch *after* reheating. In this section we assume axion or ALP oscillation *during* reheating with  $T_{\text{osc}} > T_{\text{rh}}$ . In such case, the density at present is

$$\rho_a(T_0) = \rho_a(T_{\text{osc}}) \frac{m_a}{\tilde{m}_a(T_{\text{osc}})} \frac{s(T_0)}{s(T_{\text{osc}})} \frac{S(T_{\text{osc}})}{S(T_{\text{rh}})}, \quad (4.1)$$

where the entropy dilution factor is given by

$$\begin{aligned} \frac{S(T)}{S(T_{\text{rh}})} &= \left( \frac{g_{\star s}(T)}{g_{\star s}(T_{\text{rh}})} \right) \left( \frac{T}{T_{\text{rh}}} \right)^3 \left( \frac{\mathbf{a}(T)}{\mathbf{a}_{\text{rh}}} \right)^3 = \left( \frac{g_{\star s}(T)}{g_{\star s}(T_{\text{rh}})} \right) \left( \frac{T}{T_{\text{rh}}} \right)^{\frac{3\alpha-3}{\alpha}} \\ &= \left( \frac{g_{\star s}(T)}{g_{\star s}(T_{\text{rh}})} \right) \begin{cases} \left( \frac{T_{\text{rh}}}{T} \right)^{2n+1} & \text{bosonic decay,} \\ \left( \frac{T_{\text{rh}}}{T} \right)^{\frac{7-n}{n-1}} & \text{fermionic decay,} \\ \left( \frac{T_{\text{rh}}}{T} \right)^{\frac{2n-5}{3}} & \text{bosonic annihilation.} \end{cases} \end{aligned} \quad (4.2)$$

The remaining task is to work out the oscillation temperature  $T_{\text{osc}}$  for a given  $\alpha$  parameter, or a type of reheating scenario. Note that for fermionic decay with  $n > 7$ , one has  $\alpha = 1$  as argued earlier, leading to  $S(T)/S(T_{\text{rh}}) = g_{\star s}(T)/g_{\star s}(T_{\text{rh}})$ .

## 4.1 QCD Axion

For QCD axion, there are two possibilities: Case 1:  $T_{\text{QCD}} < T_{\text{osc}}$  and Case 2:  $T_{\text{QCD}} > T_{\text{osc}}$ . In the following, we investigate these cases separately.

### 4.1.1 Case 1: $T_{\text{QCD}} < T_{\text{osc}}$

In the case with  $T_{\text{QCD}} < T_{\text{osc}}$ , axion mass features a temperature dependence:  $\tilde{m}_a = m_a(T/T_{\text{QCD}}^4)$ . Using the first line of Eq. (2.9), we work out the oscillation temperature, which is given by

$$T_{\text{osc}} = T_{\text{rh}} \left( \frac{1}{\pi} \sqrt{\frac{10}{g_\star}} \frac{m_a M_P T_{\text{QCD}}^4}{T_{\text{rh}}^6} \right)^{\frac{\alpha(2+n)}{3n+4\alpha(2+n)}}. \quad (4.3)$$

Depending on the hierarchy of the QCD scale and the reheating temperature, there are further two possibilities:  $T_{\text{rh}} < T_{\text{QCD}} < T_{\text{osc}}$  and  $T_{\text{QCD}} < T_{\text{rh}} < T_{\text{osc}}$ , which lead to constraints on reheating temperature; for the former, we have:

$$T_{\text{QCD}}^{\frac{3n}{3n-2\alpha(n+2)}} \left( \frac{1}{\pi} \sqrt{\frac{10}{g_\star}} m_a M_P \right)^{\frac{-\alpha(n+2)}{3n-2\alpha(n+2)}} < T_{\text{rh}} < T_{\text{QCD}}, \quad (4.4)$$

while the latter requires

$$T_{\text{QCD}} < T_{\text{rh}} < \left( \frac{1}{\pi} \sqrt{\frac{10}{g_\star}} m_a M_P T_{\text{QCD}}^4 \right)^{\frac{1}{6}}. \quad (4.5)$$

With the oscillation temperature Eq. (4.3) and entropy dilution factor Eq. (4.2), we can further proceed to compute the axion density Eq. (4.1), and finally the relic abundance at present.

For bosonic decay, we find a general expression in the following form<sup>6</sup>:

$$\Omega_a h^2 \simeq 0.12 \left( \frac{\theta}{1.0} \right)^2 \left( \frac{T_{\text{rh}}}{0.1 \text{ GeV}} \right)^{\frac{10-n}{n+2}} \left[ \frac{m_a}{2.59 \cdot 10^{-6} \cdot \exp\left(\frac{-20.19+3.68n}{n+4}\right) \text{ eV}} \right]^{-\frac{4+n}{n+2}}, \quad (4.6)$$

or with specific values of  $n$

$$\Omega_a h^2 \simeq 0.12 \left( \frac{\theta}{1.0} \right)^2 \begin{cases} \left( \frac{T_{\text{rh}}}{0.1 \text{ GeV}} \right)^2 \left( \frac{m_a}{3.1 \cdot 10^{-7} \text{ eV}} \right)^{-\frac{3}{2}} & \text{bosonic decay } n = 2, \\ \left( \frac{T_{\text{rh}}}{0.1 \text{ GeV}} \right)^1 \left( \frac{m_a}{1.3 \cdot 10^{-6} \text{ eV}} \right)^{-\frac{4}{3}} & \text{bosonic decay } n = 4, \\ \left( \frac{T_{\text{rh}}}{0.1 \text{ GeV}} \right)^{\frac{1}{2}} \left( \frac{m_a}{3.1 \cdot 10^{-6} \text{ eV}} \right)^{-\frac{5}{4}} & \text{bosonic decay } n = 6, \\ \left( \frac{T_{\text{rh}}}{0.1 \text{ GeV}} \right)^{\frac{1}{5}} \left( \frac{m_a}{5.6 \cdot 10^{-6} \text{ eV}} \right)^{-\frac{6}{5}} & \text{bosonic decay } n = 8. \end{cases} \quad (4.7)$$

<sup>6</sup>The exponential function ‘‘exp’’ has been introduced to make the result more compact.

Similarly, for fermionic decay, we find

$$\Omega_a h^2 \simeq 0.12 \left( \frac{\theta}{1.0} \right)^2 \begin{cases} \left( \frac{T_{\text{rh}}}{0.1 \text{ GeV}} \right)^{\frac{14-3n}{3n-2}} \left[ \frac{m_a}{1.03 \cdot 10^{-6} \cdot \exp\left(\frac{-11.64+4.61n}{n+2}\right) \text{ eV}} \right]^{\frac{3n}{2-3n}} & n < 7, \\ \left( \frac{T_{\text{rh}}}{0.1 \text{ GeV}} \right)^{\frac{7(4-n)}{8+7n}} \left[ \frac{m_a}{1.03 \cdot 10^{-6} \cdot \exp\left(\frac{-5.76+4.61n}{n+2}\right) \text{ eV}} \right]^{\frac{-7(2+n)}{8+7n}} & n > 7, \end{cases} \quad (4.8)$$

and

$$\Omega_a h^2 \simeq 0.12 \left( \frac{\theta}{1.0} \right)^2 \begin{cases} \left( \frac{T_{\text{rh}}}{0.1 \text{ GeV}} \right)^2 \left( \frac{m_a}{3.1 \cdot 10^{-7} \text{ eV}} \right)^{-\frac{3}{2}} & \text{fermionic decay } n = 2, \\ \left( \frac{T_{\text{rh}}}{0.1 \text{ GeV}} \right)^{\frac{1}{5}} \left( \frac{m_a}{5.6 \cdot 10^{-6} \text{ eV}} \right)^{-\frac{6}{5}} & \text{fermionic decay } n = 4, \\ \left( \frac{T_{\text{rh}}}{0.1 \text{ GeV}} \right)^{-\frac{1}{4}} \left( \frac{m_a}{1.5 \cdot 10^{-5} \text{ eV}} \right)^{-\frac{9}{8}} & \text{fermionic decay } n = 6, \\ \left( \frac{T_{\text{rh}}}{0.1 \text{ GeV}} \right)^{-\frac{7}{16}} \left( \frac{m_a}{2.3 \cdot 10^{-5} \text{ eV}} \right)^{-\frac{35}{32}} & \text{fermionic decay } n = 8. \end{cases} \quad (4.9)$$

For bosonic annihilation, we have

$$\Omega_a h^2 \simeq 0.12 \left( \frac{\theta}{1.0} \right)^2 \left( \frac{T_{\text{rh}}}{0.1 \text{ GeV}} \right)^{\frac{6-n}{6+n}} \left[ \frac{m_a}{1.0 \cdot 10^{-6} \cdot \exp\left(\frac{2.14+4.63n}{n+8}\right) \text{ eV}} \right]^{\frac{-(8+n)}{6+n}} \quad (4.10)$$

and

$$\Omega_a h^2 \simeq 0.12 \left( \frac{\theta}{1.0} \right)^2 \begin{cases} \left( \frac{T_{\text{rh}}}{0.1 \text{ GeV}} \right)^{\frac{1}{5}} \left( \frac{m_a}{5.6 \cdot 10^{-6} \text{ eV}} \right)^{-\frac{6}{5}} & \text{bosonic annihilation } n = 4, \\ \left( \frac{T_{\text{rh}}}{0.1 \text{ GeV}} \right)^0 \left( \frac{m_a}{8.5 \cdot 10^{-6} \text{ eV}} \right)^{-\frac{7}{6}} & \text{bosonic annihilation } n = 6, \\ \left( \frac{T_{\text{rh}}}{0.1 \text{ GeV}} \right)^{-\frac{1}{7}} \left( \frac{m_a}{1.2 \cdot 10^{-5} \text{ eV}} \right)^{-\frac{8}{7}} & \text{bosonic annihilation } n = 8. \end{cases} \quad (4.11)$$

For the scenario with  $n = 2$ , we observe that the expression for  $\Omega_a h^2$  remains the same for both the bosonic and fermionic decay reheating scenarios. This similarity arises because, in this case, the inflaton decay rate  $\Gamma$  does not exhibit time dependence due to the constant inflaton mass. Consequently, both the dilution factor Eq. (4.2) and the oscillation temperature Eq. (4.3) are identical for both bosonic and fermionic decay reheating scenarios with  $n = 2$ . Additionally, we notice that in the case of bosonic annihilation with  $n = 6$ , the relic abundance becomes independent of the reheating temperature  $T_{\text{rh}}$ , remaining the same as in the case of oscillations occurring during the radiation-dominated epoch, as shown in the second line of Eq. (3.8).

### 4.1.2 Case 2: $T_{\text{QCD}} \geq T_{\text{osc}}$

For oscillation temperature below QCD scale, we have  $\tilde{m}_a = m_a$ . Using the first line of Eq. (2.9), we find the oscillation temperature

$$T_{\text{osc}} = T_{\text{rh}} \left( \frac{1}{\pi} \sqrt{\frac{10}{g_\star}} \frac{m_a M_P}{T_{\text{rh}}^2} \right)^{\frac{\alpha(2+n)}{3n}}. \quad (4.12)$$

Similar as before, the self-consistency condition  $T_{\text{rh}} \leq T_{\text{osc}} \leq T_{\text{QCD}}$  yields bounds on reheating temperature, which in this case lead to

$$T_{\text{rh}} \leq T_{\text{QCD}}^{\frac{3n}{3n-2\alpha(2+n)}} \left( \frac{1}{\pi} \sqrt{\frac{10}{g_\star}} m_a M_P \right)^{\frac{-\alpha(2+n)}{3n-2\alpha(2+n)}}; \quad (4.13)$$

$$T_{\text{rh}} \leq \left( \frac{1}{\pi} \sqrt{\frac{10}{g_\star}} m_a M_P \right)^{\frac{1}{2}}. \quad (4.14)$$

With the oscillation temperature, we find the relic abundance reads

$$\Omega_a h^2 \simeq 0.12 \left( \frac{\theta}{1.0} \right)^2 \left( \frac{T_{\text{rh}}}{4 \text{ MeV}} \right)^{\frac{4-n}{n}} \left[ \frac{m_a}{1.0 \cdot 10^{-6} \cdot \exp\left(\frac{-35.29+7.85 n}{n+2}\right) \text{ eV}} \right]^{-\frac{2+n}{n}}, \quad (4.15)$$

or with specific value of  $n$ :

$$\Omega_a h^2 \simeq 0.12 \left( \frac{\theta}{1.0} \right)^2 \begin{cases} \left( \frac{T_{\text{rh}}}{4 \text{ MeV}} \right)^1 \left( \frac{m_a}{7.5 \cdot 10^{-9} \text{ eV}} \right)^{-2} & n = 2, \\ \left( \frac{T_{\text{rh}}}{4 \text{ MeV}} \right)^0 \left( \frac{m_a}{5.2 \cdot 10^{-7} \text{ eV}} \right)^{-\frac{3}{2}} & n = 4, \\ \left( \frac{T_{\text{rh}}}{4 \text{ MeV}} \right)^{-\frac{1}{3}} \left( \frac{m_a}{4.4 \cdot 10^{-6} \text{ eV}} \right)^{-\frac{4}{3}} & n = 6, \\ \left( \frac{T_{\text{rh}}}{4 \text{ MeV}} \right)^{-\frac{1}{2}} \left( \frac{m_a}{1.6 \cdot 10^{-5} \text{ eV}} \right)^{-\frac{5}{4}} & n = 8. \end{cases} \quad (4.16)$$

It is interesting to note that the relic abundance is independent of the  $\alpha$  parameter or the form of inflaton-matter couplings, even though the oscillation temperature still depends on them. This becomes clear to recall from Eq. (4.1) that

$$\rho_a(T_0) \propto \frac{1}{T_{\text{osc}}^3} \left( \frac{T_{\text{osc}}}{T_{\text{rh}}} \right)^{\frac{3\alpha-3}{\alpha}} = T_{\text{rh}}^{\frac{3-3\alpha}{\alpha}} T_{\text{osc}}^{-\frac{3}{\alpha}} \propto T_{\text{rh}}^{\frac{4-n}{n}} m_a^{-\frac{n+2}{n}}, \quad (4.17)$$

where we have utilized Eq. (4.12) to rewrite  $T_{\text{osc}}$  with  $m_a$  and  $T_{\text{rh}}$  in the last step. We also notice that for  $n = 4$ , the relic abundance is independent from the reheating  $T_{\text{rh}}$ , being the same as the first line of Eq. (3.8).

In Fig. 1, we illustrate the parameter space  $(T_{\text{rh}}, m_a)$  or  $(T_{\text{rh}}, f_a)$  that gives rise to the observed DM relic abundance. The blue lines, depicted as solid, dashed, dash-dotted, and dotted, correspond to different values of  $n$ , specifically  $n = 2, 4, 6$  and  $8$ , respectively. The

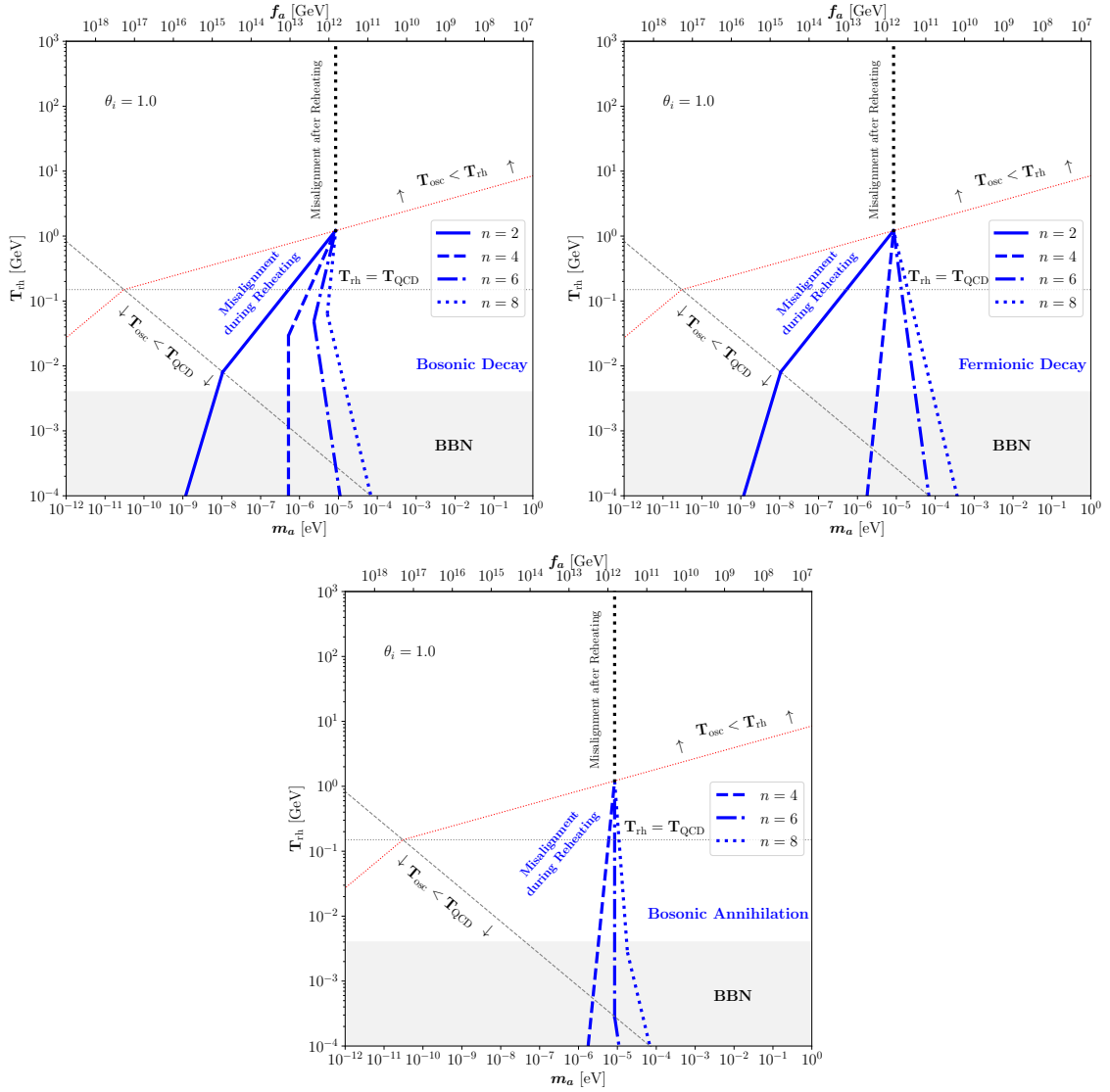


**Figure 1.** Blue lines correspond to  $T_{\text{rh}}$  as function of  $m_a$  (or  $f_a$ ) generating the observed axion DM relic density for bosonic (upper left), fermionic (upper right) inflaton decay and bosonic inflaton annihilation (lower panel) with different  $n$  and  $\theta_i = 1$ .

red dotted line corresponds to  $T_{\text{rh}} = T_{\text{osc}}$ , which divides the parameter space into regions of  $T_{\text{rh}} > T_{\text{osc}}$  and  $T_{\text{rh}} < T_{\text{osc}}$ , above and below it, respectively. The vertical black dotted line represents the scenario with  $T_{\text{rh}} > T_{\text{osc}}$ , where oscillations occur *after* reheating, specifically during the radiation epoch, with  $m_a \simeq 8.6 \cdot 10^{-6} \text{eV}$ . The horizontal gray dotted line denotes  $T_{\text{rh}} = T_{\text{QCD}}$ . The gray dashed line symbolizes  $T_{\text{osc}} = T_{\text{QCD}}$ , marking the boundary between regions of  $T_{\text{osc}} < T_{\text{QCD}}$  and  $T_{\text{osc}} > T_{\text{QCD}}$ . Note that  $T_{\text{osc}}$  depends on both  $n$  and  $\alpha$  (or the type of inflaton-matter couplings). For a fixed  $n$ , the proximity of  $T_{\text{osc}}$  to  $T_{\text{QCD}}$  leads to a change in slope for the blue lines, an effect attributed to the temperature-dependent nature of the axion mass. In the plot, we only depict  $T_{\text{osc}} = T_{\text{QCD}}$  (gray dashed line) with  $n = 2$  for

bosonic decay (upper left panel) and fermionic decay (upper right panel), and with  $n = 6$  for bosonic annihilation (lower panel). For the fermionic decay with  $n > 2$  and bosonic annihilation with  $n = 4$ , the blue lines change slopes at regimes with much smaller  $T_{\text{rh}}$ , which are not visible in the figure. Lastly, the shaded gray band characterizes  $T_{\text{rh}} \lesssim 4 \text{ MeV}$ , a range contradictory to the requirements of Big Bang nucleosynthesis (BBN) [86, 87], and therefore disfavored.

In the scenario where  $n = 2$ , we observe that the parameter space remains identical for both bosonic and fermionic decay modes, as explained before. In this context, the axion mass can reach remarkably small values, approximately  $m_a \simeq 7.5 \cdot 10^{-9} \text{ eV}$ , assuming  $T_{\text{rh}} \simeq 4 \text{ MeV}$  and  $\theta_i = 1.0$ . By further reducing  $\theta_i$ , the lower limit of  $m_a$  can be pushed even lower. For example, with  $\theta_i = 0.5$ , the axion mass can be as small as  $m_a \simeq 3.7 \cdot 10^{-9} \text{ eV}$  while maintaining  $T_{\text{rh}} \simeq 4 \text{ MeV}$ . Conversely, if we explore larger misalignment angles, such as  $\theta_i = \pi/\sqrt{3}$ , and higher reheating temperatures, around  $T_{\text{rh}} \simeq 1 \text{ GeV}$ , we find that the axion mass increases, reaching approximately  $m_a \simeq 2.4 \cdot 10^{-5} \text{ eV}$ . These results for  $n = 2$  align with the early matter case discussed in Ref. [42].

As we examine larger values of  $n$  (while keeping  $T_{\text{rh}}$  constant), an intriguing trend emerges. The dilution factor, as presented in Eq. (4.2), tends to grow, leading to an increased demand for a larger axion mass to satisfy the condition that the axion density at present is fixed. This elucidates the ordering of the blue curves (from left to right) within the parameter space. Although we are focusing on the regime with  $n \leq 8$ , it is still interesting to note that in the limit  $n \rightarrow \infty$ , axion mass can be as large as  $\mathcal{O}(10^{-2}) \text{ eV}$  (cf. Eq. (4.15)). This upper bound on axion mass is in agreement with scenarios where oscillations occur during the kination epoch [42].

With the increase of the reheating temperature  $T_{\text{rh}}$ , we notice that the blue lines tend to merge to the black dotted line. The physical reason is that for larger  $T_{\text{rh}}$ , misalignment tends to occur *after* reheating so that the effect of details of reheating dynamics do not play a role. Using Eq. (4.14), and  $m_a \simeq 8.6 \cdot 10^{-6} \text{ eV}$ , we find an upper bound on reheating temperature:

$$T_{\text{rh}} \lesssim 1 \text{ GeV}, \quad (4.18)$$

which guarantees that misalignment happens during reheating.

An intriguing feature of Fig. 1 is that the distinctions among different reheating scenarios as well as their effects on the extended parameter space become pronounced for  $n > 2$ , which contribute to the distinct shapes of the curves as depicted in the three figures. As a result, we have different ranges of axion mass for a given reheating temperature  $T_{\text{rh}} \lesssim 1 \text{ GeV}$  in the different reheating scenarios.

So far, we have only focused on  $\theta_i = 1.0$ . In Table 1, we explore the parameter space concerning the axion mass  $m_a$  for various reheating scenarios and specific values of  $n$  by allowing wider range of initial misalignment angle:  $\theta_i \in [0.5, \pi/\sqrt{3}]$ . In the bosonic annihilation scenario, we leave it empty for  $n = 2$  since it is not possible to have successful reheating with inflaton annihilation alone. Again, one can see that the parameter space can vary for different reheating scenarios. In particular, the bosonic annihilation scenarios do *not* allow axion mass in the regime:  $3.7 \cdot 10^{-9} \text{ eV} \lesssim m_a \lesssim 5.1 \cdot 10^{-7} \text{ eV}$ , which is nevertheless

$m_a/\text{eV}$ \diagdown scenario	Ferminionic Decay	Bosonic Decay	Bosonic Annihilation
$n = 2$	$[3.7 \cdot 10^{-9}, 2.4 \cdot 10^{-5}]$	$[3.7 \cdot 10^{-9}, 2.4 \cdot 10^{-5}]$	
$n = 4$	$[5.1 \cdot 10^{-7}, 2.4 \cdot 10^{-5}]$	$[2.1 \cdot 10^{-7}, 2.4 \cdot 10^{-5}]$	$[5.1 \cdot 10^{-7}, 2.4 \cdot 10^{-5}]$
$n = 6$	$[2.6 \cdot 10^{-6}, 8.7 \cdot 10^{-5}]$	$[1.6 \cdot 10^{-6}, 2.4 \cdot 10^{-5}]$	$[2.6 \cdot 10^{-6}, 2.4 \cdot 10^{-5}]$
$n = 8$	$[2.6 \cdot 10^{-6}, 2.5 \cdot 10^{-4}]$	$[2.6 \cdot 10^{-6}, 4.1 \cdot 10^{-5}]$	$[2.6 \cdot 10^{-6}, 4.9 \cdot 10^{-5}]$

**Table 1.** Summary of parameter space of  $m_a$  for QCD axion DM in a different reheating scenario with  $\theta_i \in [0.5, \pi/\sqrt{3}]$  and  $4 \text{ MeV} \lesssim T_{\text{rh}} \lesssim 1 \text{ GeV}$ .

supported in the decay scenarios. It is also interesting to note that only fermionic decay scenarios can give rise to  $4.9 \cdot 10^{-5} \text{ eV} \lesssim m_a \lesssim 2.5 \cdot 10^{-4} \text{ eV}$ . These distinctions in the parameter space have very important experimental implications, as will be explored in Sec. 5.

## 4.2 ALP

So far, we have only focused on the QCD axions. In this section, we shift our focus to the axion-like particles (ALPs). When oscillations happen *during* reheating, the oscillation temperature is the same as the expression given in Eq. (4.3). The allowed reheating temperature in this case reads

$$4 \text{ MeV} \leq T_{\text{rh}} \leq T_{\text{osc}} \simeq \left( \frac{1}{\pi} \sqrt{\frac{10}{g_\star}} m_a M_P \right)^{\frac{1}{2}}, \quad (4.19)$$

which leads to a lower bound on ALP mass:

$$m_a \gtrsim 2.2 \cdot 10^{-14} \text{ eV}. \quad (4.20)$$

Here we assume that ALP mass to be a constant in time, and the ALP energy density is then given by

$$\rho_a(T_0) = \rho_a(T_{\text{osc}}) \frac{s(T_0)}{s(T_{\text{osc}})} \frac{S(T_{\text{osc}})}{S(T_{\text{rh}})} \simeq \frac{1}{2} m_a^2 f_a^2 \theta_i^2 \frac{s(T_0)}{s(T_{\text{osc}})} \frac{S(T_{\text{osc}})}{S(T_{\text{rh}})}, \quad (4.21)$$

where the entropy dilution factor  $S(T_{\text{osc}})/S(T_{\text{rh}})$  can be computed using Eq. (4.2). This leads to:

$$\Omega_a h^2 \simeq \left( \frac{\theta_i}{1.0} \right)^2 \left( \frac{f_a}{1.3 \cdot 10^{13} \cdot \exp(8.1/n) \text{ GeV}} \right)^2 \left( \frac{T_{\text{rh}}}{4 \text{ MeV}} \right)^{\frac{4-n}{n}} \left( \frac{m_a}{7.4 \cdot 10^{-11} \text{ eV}} \right)^{\frac{n-2}{n}}, \quad (4.22)$$

or in specific value of  $n$ :

$$\Omega_a h^2 \simeq \left(\frac{\theta_i}{1.0}\right)^2 \begin{cases} \left(\frac{f_a}{7.6 \cdot 10^{14} \text{ GeV}}\right)^2 \left(\frac{T_{\text{rh}}}{4 \text{ MeV}}\right)^1 \left(\frac{m_a}{7.4 \cdot 10^{-11} \text{ eV}}\right)^0 & n = 2, \\ \left(\frac{f_a}{1.0 \cdot 10^{14} \text{ GeV}}\right)^2 \left(\frac{T_{\text{rh}}}{4 \text{ MeV}}\right)^0 \left(\frac{m_a}{7.4 \cdot 10^{-11} \text{ eV}}\right)^{\frac{1}{2}} & n = 4, \\ \left(\frac{f_a}{5.1 \cdot 10^{13} \text{ GeV}}\right)^2 \left(\frac{T_{\text{rh}}}{4 \text{ MeV}}\right)^{-\frac{1}{3}} \left(\frac{m_a}{7.4 \cdot 10^{-11} \text{ eV}}\right)^{\frac{2}{3}} & n = 6, \\ \left(\frac{f_a}{3.6 \cdot 10^{13} \text{ GeV}}\right)^2 \left(\frac{T_{\text{rh}}}{4 \text{ MeV}}\right)^{-\frac{1}{2}} \left(\frac{m_a}{7.4 \cdot 10^{-11} \text{ eV}}\right)^{\frac{3}{4}} & n = 8. \end{cases} \quad (4.23)$$

As a means of cross checking and to ensure the consistency of our analysis, we note that Eq. (4.22) and Eq. (4.23) reproduce Eq. (4.15) and Eq. (4.16) once replacing  $f_a$  to  $m_a$  by using Eq. (3.1). Similar to the case with  $T_{\text{osc}} < T_{\text{QCD}}$  for QCD axion, we find that the parameter space remains unaffected by the type of inflaton-matter couplings under consideration.

Our results in this section become particularly interesting when examining different values of  $n$  within the context of ALPs. Starting with the case where  $n = 2$ , our analysis aligns with the results presented in Ref. [40], where the authors study ALPs misalignment during early matter domination. We confirm that  $\Omega_a h^2$  remains independent of  $m_a$ , thereby resulting in the relationship  $f_a \propto T_{\text{rh}}^{-1/2}$  as a prerequisite for achieving the observed DM relic abundance. Another scenario, outlined in Ref. [40], corresponds to the limit of  $n \rightarrow \infty$ , where we find that  $f_a \propto m_a^{-1}$  holds true. Our results for  $n = 2$  and  $n \rightarrow \infty$  thus stand as a validation of the earlier work.

Being complementary to Ref. [40], we explore additional values of  $n$ , revealing the trends as follows.

- For  $n = 4$ ,  $\Omega_a h^2$  becomes independent of  $T_{\text{rh}}$ , mirroring the scenario where ALP oscillates during the radiation epoch (cf. Eq. (3.10)). Consequently, to account for the observed DM relic abundance, the requirement shifts to  $f_a \propto m_a^{-1/4}$ .
- When considering  $n > 4$ , we delve into a domain where  $f_a$  can be significantly smaller than what would be necessary under radiation-like oscillation conditions. For instance, for  $n = 6$ , we ascertain that  $f_a \propto m_a^{-1/3}$ , while for  $n = 8$ , the relationship shifts to  $f_a \propto m_a^{-3/8}$ .

This intriguing range of  $n$  values leads to interesting experimental implications that will be explored in the forthcoming section.

## 5 Experimental Constraints

In previous sections, we have worked out the parameter space for QCD axion and ALP misalignment *during* reheating. We have shown that the parameter space can be enlarged and show distinct features for different reheating scenarios. In this section, we are devoted to investigating the experimental constraints and implications.

As a benchmark scenario, we consider axions and ALPs couple to two photons via an effective dimension-5 operator [22–24, 88]:

$$\mathcal{L}_{a\gamma} = -\frac{1}{4} g_{a\gamma} a F_{\mu\nu} \tilde{F}^{\mu\nu} = g_{a\gamma} a \vec{E} \cdot \vec{B}, \quad (5.1)$$

where  $g_{a\gamma}$  corresponds to the coupling constant. It is related to the decay constant as [88]

$$g_{a\gamma} \simeq 10^{-13} \text{ GeV}^{-1} \left( \frac{10^{10} \text{ GeV}}{f_a} \right). \quad (5.2)$$

In the landscape of experimental constraints, numerous developments have emerged to shed light on the axion and ALP parameter space [62, 63, 88]. Within this context, our primary focus centers on specific experimental endeavors, particularly Haloscope and Telescope experiments, which are relevant to the parameter space of interest in this article. Here we briefly mention several relevant experiments, including some ongoing Haloscope experiments, e.g. ADMX [89–93] and CAPP [94–98] and Telescope experiments e.g. MUSE [99]. The sensitivity regimes are depicted in dark gray color. We also consider some future projection limits in gray dashed lines from several Haloscope experiments aimed for different mass regimes. These include DM-Radio for  $m_a$  in 20 – 800 neV [100], FLASH for  $m_a$  in 0.2 – 1  $\mu\text{eV}$  [101], Baby-IAIXO for  $m_a$  in 1 – 2  $\mu\text{eV}$  [102], ADMX for  $m_a$  in 1.9 – 3.7  $\mu\text{eV}$  [103], QUAX for  $m_a$  in 35 – 45  $\mu\text{eV}$ , DALI for  $m_a$  in 20 – 250  $\mu\text{eV}$  [104], ALPHA for  $m_a$  in 35 – 400  $\mu\text{eV}$  [105], MADMAX for  $m_a$  in 40 – 400  $\mu\text{eV}$  [106], ORGAN for  $m_a$  in 60 – 210  $\mu\text{eV}$  [107], CADEX for  $m_a$  in 330 – 460  $\mu\text{eV}$  [108], BRASS for  $m_a$  in 10 – 104 meV, BREAD for  $m_a$  in  $10^{-3}$  – 1 eV [109], LAMPOST for  $m_a$  in 0.1 – 10 eV [110]. These constraints and projection curves have been generated by using the AxionLimits code in [111].

## 5.1 Results

In Fig. 2, we present the parameter space ( $g_{a\gamma}, m_a$ ) that leads to the correct relic abundance. The black dotted line represents the prediction for the QCD axion using Eq. (3.1) and Eq. (5.2). It is important to note that not all points along this line fulfill the condition for axions to produce the correct relic abundance. For the scenario where oscillations occur during the radiation epoch *after* reheating, we find specific values that match this requirement:  $m_a \simeq 2.4 \cdot 10^{-5}$  eV and  $g_{a\gamma} \simeq 4.1 \cdot 10^{-15}$   $\text{GeV}^{-1}$  with  $\theta_i = \pi/\sqrt{3}$ . This specific point is illustrated as the red dot on the plot. It is worth mentioning that the parameter space can be expanded further if the misalignment takes place *during* the reheating phase, as thoroughly investigated in the previous section.

The upper left, upper right, and lower panels of the figure correspond to distinct reheating scenarios achieved via inflaton fermionic decay, inflaton bosonic decay, and bosonic annihilation, respectively. In each panel, the blue lines delineate the parameter space where the QCD axion can account for dark matter, specifically when oscillations occur *during* the reheating phase. The segments between red dot and other dots of various colors, namely black, blue, green, and magenta, delineate the regions where the conditions for the observed relic abundance are satisfied for different values of  $n$  ( $n = 2, n = 4, n = 6, \text{ and } n = 8$ ). The gray vertical dotted lines in all panels correspond to the lower and upper limits on  $m_a$  as outlined in Table 1.

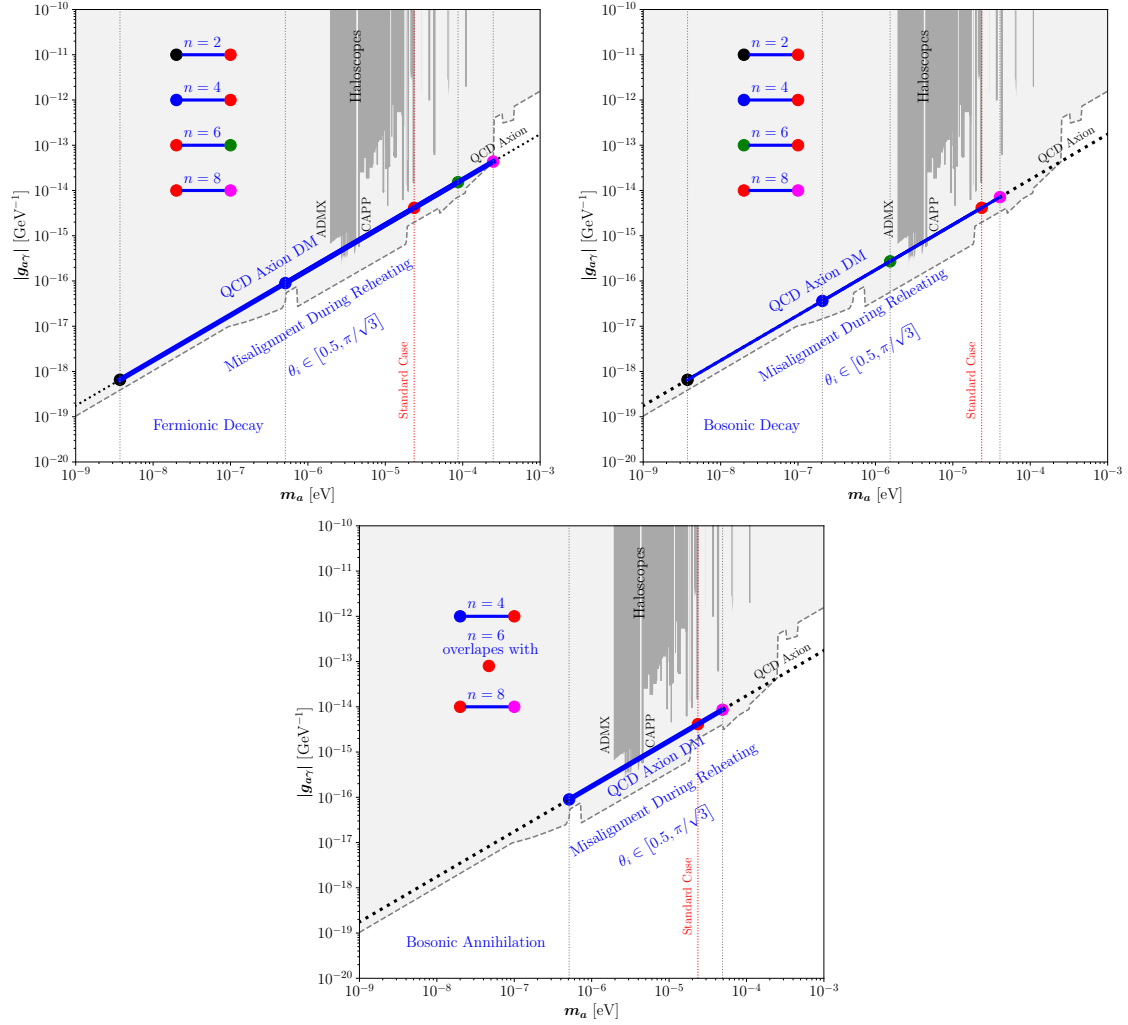


**Figure 2.** The blue lines correspond to the parameter space with  $g_{a\gamma}$  as function of  $m_a$  to yield correct DM relic abundance for QCD axion by assuming misalignment occurs *during* reheating. The red dot corresponds to the standard case where oscillation occurs in radiation epoch *after* reheating with  $\theta_i = \pi/\sqrt{3}$ . The segments between red and black, red and blue, red and green, red and magenta dots correspond to the parameter space with  $n = 2$ ,  $n = 4$ ,  $n = 6$ , and  $n = 8$ , respectively. For bosonic annihilation,  $n = 6$  overlaps with the standard case (red dot). The constraints (dark grey region) and future projection limits (grey dashed lines) are generated by using the AxionLimits code [111].

We have considered the initial misalignment angle as  $\theta_i \in [0.5, \pi/\sqrt{3}]$  in all panels. It is interesting to notice that a portion of the extended parameter space are already constrained by the Haloscope experiments, for example ADMX [89–93] and CAPP [94–98]. Depending on the underlying reheating scenarios, the conclusions differ as will be explained in the following.

- Fermionic Decay Scenario.

For the reheating scenario through inflaton fermionic decay, we observe that the pa-

parameter space corresponding to  $n = 2$  and  $n = 4$  is susceptible to sensitivity by ADMX and CAPP experiments. Notably, regions within the axion mass range of  $2 \cdot 10^{-6}$  eV to  $5 \cdot 10^{-6}$  eV are already ruled out by these experiments, as depicted in the upper left panel of Fig. 2. However, for  $n > 4$ , the current Haloscope experiments are less likely to probe the parameter space associated with the reheating scenario via fermionic decay.

- **Bosonic Decay Scenario.**

Within the context of the bosonic decay scenario, the results are different compared to previous fermionic decay scenarios. Specifically, the current ADMX and CAPP experiments are sensitive to the scenarios with  $n \leq 6$ .

- **Bosonic Annihilation Scenario.**

In the context of the bosonic annihilation scenario with  $n = 6$ , the parameter space overlaps with the case of oscillations during the radiation epoch. The parameter space for  $n = 4$  is identical to that in the fermionic decay scenario and is slightly larger than that in the bosonic decay scenario for  $n = 8$ , which is also shown in Table 1. It is evident that only the scenario with  $n = 4$  is constrained with the current ADMX and CAPP experiments.

In Fig. 3, we illustrate the relationship between  $(g_{a\gamma}, m_a)$  that results in the correct relic abundance for ALPs, with a focus on its dependence on the parameter  $n$ . We have fixed  $\theta_i \in [0.5, \pi/\sqrt{3}]$  and  $T_{\text{rh}} = 4$  MeV, and considered the ALP mass bound presented in Eq. (4.20), as we are mainly focusing on misalignment during reheating.

The magenta, blue, green and red shaded bands correspond to different values of  $n$ , specifically  $n = 2$ ,  $n = 4$ ,  $n = 6$ , and  $n = 8$ , respectively. For fixed  $m_a$  and reheating temperature  $T_{\text{rh}}$ , with increasing values of  $n$ , a smaller decay constant  $f_a$  is required (cf. Eq. (4.23)), which in turn leads to a larger value of the axion-photon coupling constant  $g_{a\gamma}$ . Consequently, the parameter space corresponding to higher values of  $n$  becomes more accessible for probing. For larger reheating temperature, the red band with  $n = 8$  and green band with  $n = 6$  move downwards, while the magenta band with  $n = 2$  moves upwards. Note that the case with  $n = 4$  is identical to the scenario where oscillations occur during the radiation epoch, being independent of  $T_{\text{rh}}$ .

An intriguing observation emerges when considering the impact of ongoing experiments. For  $n = 8$ , current Haloscope experiments, such as ADMX and CAPP, have already constrained the parameter space within the axion mass range of  $2 \cdot 10^{-6}$  eV to  $5 \cdot 10^{-6}$  eV. Additionally, Telescope experiments, like MUSE [99], are capable of constraining the parameter space with  $2.7$  eV  $\lesssim m_a \lesssim 5.3$  eV for this case. As  $n$  decreases, for instance in the case of  $n = 6$ , the parameter space moves beyond the sensitivity of MUSE but can still be probed through ADMX and CAPP experiments. For  $n = 4$  and  $n = 2$ , the parameter space extends beyond the reach of current ADMX and CAPP experiments, resulting in a different conclusion compared to the scenario of QCD axions.

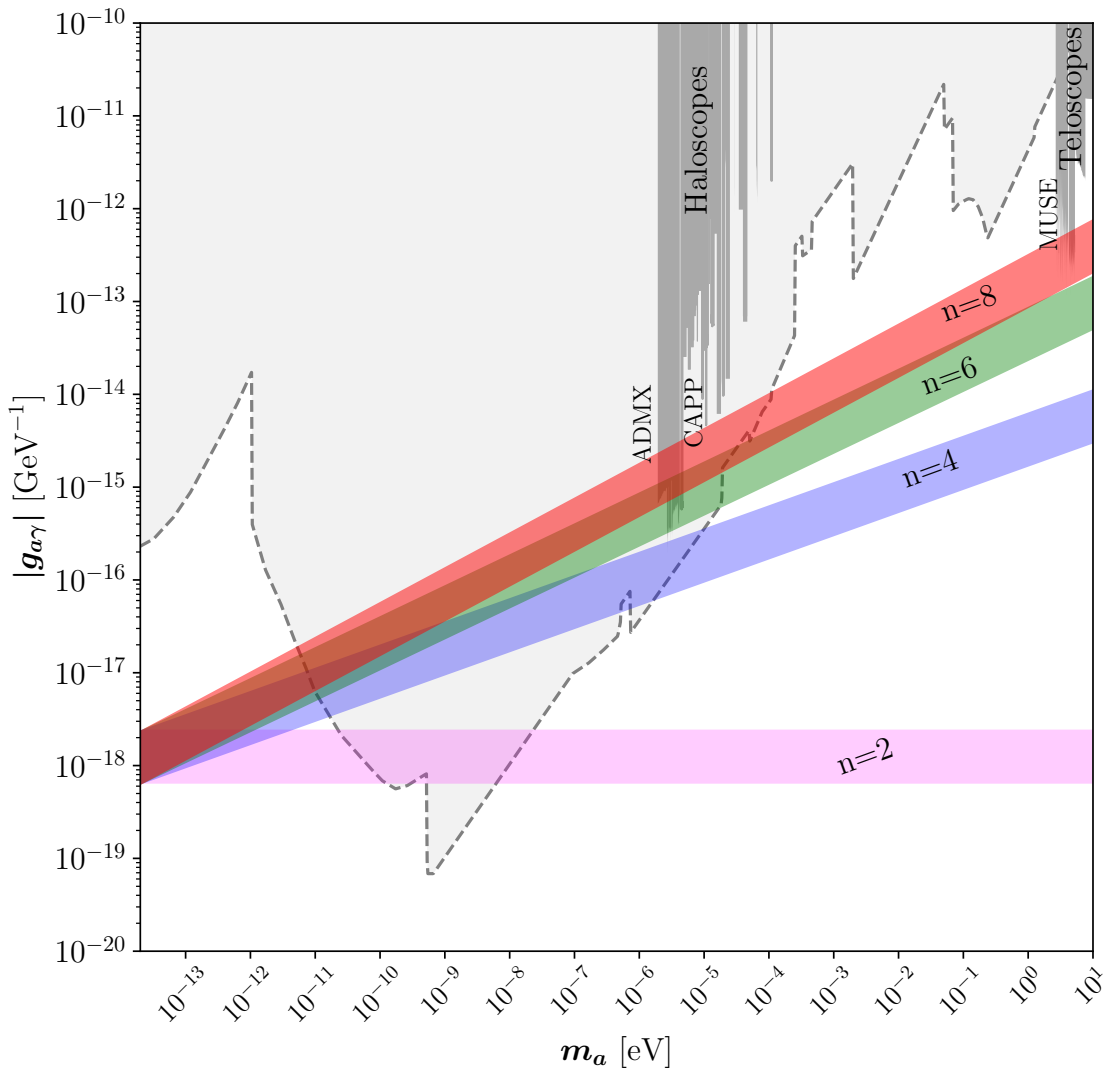


**Figure 3.** Colored bands correspond to the parameter space for  $g_{a\gamma}$  as function of  $m_a$  to yield correct ALP DM relic abundance by assuming misalignment occurs *during* reheating with different values of  $n$ . We have considered  $\theta_i \in [0.5, \pi/\sqrt{3}]$  and  $T_{\text{rh}} = 4$  MeV. The scenario with  $n = 4$  is identical to the standard case where oscillations occur during the radiation epoch. The current constraints (dark grey regimes) and future projection limits (grey dashed lines) are generated by using the AxionLimits code [111].

## 5.2 Probing Reheating via Axion Experiments

Given the distinct behaviors of the parameter space and the resultant constraints arising from different reheating scenarios, it is possible that future axion experiments hold considerable potential for constraining the reheating process. Here, we offer insights into how these experiments could play a role in constraining the reheating dynamics.

For the QCD axion, it is evident from Fig. 2 that future Haloscope experiments have the potential to constrain the extended parameter space associated with the considered re-

heating scenarios. If these experiments detect positive signals, they would provide valuable constraints on the reheating mechanisms. For instance, if a signal is observed in the lower mass regime:  $3.7 \cdot 10^{-9} \text{ eV} \lesssim m_a \lesssim 5.1 \cdot 10^{-7} \text{ eV}$  (cf. Table 1), this would suggest that the reheating scenario via bosonic annihilation becomes less likely. Similarly, if a signal emerges in a larger mass range:  $4.9 \cdot 10^{-5} \text{ eV} \lesssim m_a \lesssim 2.5 \cdot 10^{-4} \text{ eV}$  (cf. Table 1), the reheating scenarios involving bosonic decay and annihilation with  $n \lesssim 8$  could be ruled out. This exclusion could be achieved without necessitating a fine-tuning of the misalignment angle.

For ALPs, a portion of the parameter space can be probed by future Haloscope experiments, as indicated in Fig. 3. However, it is important to note that the larger mass region remains outside the sensitivity of these experiments. Due to the distinct ordering of parameter space for different  $n$  values, future experiments are particularly sensitive to scenarios with higher values of  $n$ . Consequently, if a signal is detected in the larger mass region, it could lead to the exclusion of scenarios with smaller values of  $n$ . Unlike the QCD axion case, the underlying type of inflaton-matter couplings cannot be readily deduced from these observations in the context of ALPs.

## 6 Conclusions

In this work, we investigated the production of QCD axions and axion-like particles (ALPs) as candidates for dark matter (DM) via the vacuum misalignment mechanism *during* inflationary reheating. By assuming that the inflaton oscillates around a generic monomial potential  $\sim \phi^n$ , we derived the parameter space that gives rise to the correct relic abundance for reheating scenarios involving inflaton decay and annihilation. Additionally, we explored the experimental constraints by comparing the parameter space with current and future axion experiments.

For QCD axions with  $T_{\text{osc}} > T_{\text{QCD}}$ , our analysis in Sec. 4.1.1 revealed a dependence of relic abundance on both the value of  $n$  and the type of inflaton-matter couplings. In the contrasting scenario of  $T_{\text{osc}} < T_{\text{QCD}}$ , as elucidated in Sec. 4.1.2, the relic abundance was shown to hinge solely on the value of  $n$ . Notably, we demonstrated that for reheating temperatures  $4 \text{ MeV} \lesssim T_{\text{rh}} \lesssim 1 \text{ GeV}$ , the parameter space capable of yielding the correct relic abundance can be significantly expanded compared to the conventional case where misalignment transpires in the radiation-dominated epoch *after* reheating. This augmentation is depicted in Fig. 1 and summarized in Table 1. For ALPs, we found that the parameter space can also be extended and is influenced only by the value of  $n$ . We derived several general analytical expressions, such as Eq. (4.22) and Eq. (4.15), which can reproduce the earlier results [40, 42] concerning misalignment during early matter ( $n = 2$ ) and kination epochs ( $n \rightarrow \infty$ ).

By further considering axion and ALP couplings to photons, we examined the constraints imposed by current and future experiments. Due to the dependence of the enlarged parameter space on the underlying reheating dynamics, the constraints differ for different reheating scenarios. For QCD axions, we found that current ADMX and CAPP experiments are already capable of ruling out certain parts of the expanded parameter space with  $2 \cdot 10^{-6} \text{ eV} \lesssim m_a \lesssim 5 \cdot 10^{-6} \text{ eV}$ , particularly when  $n \leq 4$  for both the decay and

annihilation scenarios. For  $n = 6$ , we found that ADMX and CAPP experiments exhibit the potential to probe  $m_a \sim 5 \cdot 10^{-6}$  eV solely in the context of bosonic decay scenario. These results are shown in Fig. 2. For ALPs, our analysis identified Telescope experiments like MUSE are already capable of constraining scenarios involving  $n = 8$  in the mass range of 2.7 eV – 5.3 eV, as depicted in Fig. 3.

By mapping the extended parameter space with future experimental projections, we found that forthcoming Haloscope experiments hold significant potential to constrain the parameter space associated with different reheating scenarios for both QCD axions and ALPs. We also highlighted that positive detections at certain mass regimes could lead to exclusion of specific reheating scenarios. In particular, by assuming QCD axions as DM, we found that the bosonic annihilation reheating scenarios become less likely if a signal is observed in the lower mass regime:  $3.7 \cdot 10^{-9}$  eV  $\lesssim m_a \lesssim 5.1 \cdot 10^{-7}$  eV. On the other hand, if a signal were to appear within a range with larger mass:  $4.9 \cdot 10^{-5}$  eV  $\lesssim m_a \lesssim 2.5 \cdot 10^{-4}$  eV, the reheating scenarios involving bosonic decay and annihilation with  $n \lesssim 8$  could be ruled out, unless the initial misalignment angle is not  $\mathcal{O}(1)$ .

## Acknowledgments

The author is grateful to Nicolás Bernal and Manuel Drees for comments on the draft. YX receives support from the Cluster of Excellence “Precision Physics, Fundamental Interactions, and Structure of Matter” (PRISMA+ EXC 2118/1) funded by the Deutsche Forschungsgemeinschaft (DFG, German Research Foundation) within the German Excellence Strategy (Project No. 39083149).

## References

- [1] J. Preskill, M.B. Wise and F. Wilczek, *Cosmology of the Invisible Axion*, *Phys. Lett. B* **120** (1983) 127.
- [2] L.F. Abbott and P. Sikivie, *A Cosmological Bound on the Invisible Axion*, *Phys. Lett. B* **120** (1983) 133.
- [3] M. Dine and W. Fischler, *The Not So Harmless Axion*, *Phys. Lett. B* **120** (1983) 137.
- [4] P. Arias, D. Cadamuro, M. Goodsell, J. Jaeckel, J. Redondo and A. Ringwald, *WISPy Cold Dark Matter*, *JCAP* **06** (2012) 013 [[1201.5902](#)].
- [5] R.D. Peccei and H.R. Quinn, *CP Conservation in the Presence of Instantons*, *Phys. Rev. Lett.* **38** (1977) 1440.
- [6] R.D. Peccei and H.R. Quinn, *Constraints Imposed by CP Conservation in the Presence of Instantons*, *Phys. Rev. D* **16** (1977) 1791.
- [7] S. Weinberg, *A New Light Boson?*, *Phys. Rev. Lett.* **40** (1978) 223.
- [8] F. Wilczek, *Problem of Strong P and T Invariance in the Presence of Instantons*, *Phys. Rev. Lett.* **40** (1978) 279.
- [9] J.P. Conlon, *The QCD axion and moduli stabilisation*, *JHEP* **05** (2006) 078 [[hep-th/0602233](#)].

- [10] P. Svrcek and E. Witten, *Axions In String Theory*, *JHEP* **06** (2006) 051 [[hep-th/0605206](#)].
- [11] A. Arvanitaki, S. Dimopoulos, S. Dubovsky, N. Kaloper and J. March-Russell, *String Axiverse*, *Phys. Rev. D* **81** (2010) 123530 [[0905.4720](#)].
- [12] B.S. Acharya, K. Bobkov and P. Kumar, *An M Theory Solution to the Strong CP Problem and Constraints on the Axiverse*, *JHEP* **11** (2010) 105 [[1004.5138](#)].
- [13] M. Cicoli, M. Goodsell and A. Ringwald, *The type IIB string axiverse and its low-energy phenomenology*, *JHEP* **10** (2012) 146 [[1206.0819](#)].
- [14] K. Choi, S.H. Im and C. Sub Shin, *Recent Progress in the Physics of Axions and Axion-Like Particles*, *Ann. Rev. Nucl. Part. Sci.* **71** (2021) 225 [[2012.05029](#)].
- [15] P. Agrawal, K.V. Berghaus, J. Fan, A. Hook, G. Marques-Tavares and T. Rudelius, *Some open questions in axion theory*, in *Snowmass 2021*, 3, 2022 [[2203.08026](#)].
- [16] P. Sikivie, *Axion Cosmology*, *Lect. Notes Phys.* **741** (2008) 19 [[astro-ph/0610440](#)].
- [17] N. Bernal, F. Hajkarim and Y. Xu, *Axion Dark Matter in the Time of Primordial Black Holes*, *Phys. Rev. D* **104** (2021) 075007 [[2107.13575](#)].
- [18] F. Schiavone, D. Montanino, A. Mirizzi and F. Capozzi, *Axion-like particles from primordial black holes shining through the Universe*, *JCAP* **08** (2021) 063 [[2107.03420](#)].
- [19] N. Bernal, Y.F. Perez-Gonzalez, Y. Xu and O. Zapata, *ALP dark matter in a primordial black hole dominated universe*, *Phys. Rev. D* **104** (2021) 123536 [[2110.04312](#)].
- [20] K. Mazde and L. Visinelli, *The interplay between the dark matter axion and primordial black holes*, *JCAP* **01** (2023) 021 [[2209.14307](#)].
- [21] M.S. Turner, *Windows on the Axion*, *Phys. Rept.* **197** (1990) 67.
- [22] D.J.E. Marsh, *Axion Cosmology*, *Phys. Rept.* **643** (2016) 1 [[1510.07633](#)].
- [23] L. Di Luzio, M. Giannotti, E. Nardi and L. Visinelli, *The landscape of QCD axion models*, *Phys. Rept.* **870** (2020) 1 [[2003.01100](#)].
- [24] P. Sikivie, *Invisible Axion Search Methods*, *Rev. Mod. Phys.* **93** (2021) 015004 [[2003.02206](#)].
- [25] E.W. Kolb and M.S. Turner, *The Early Universe*, vol. 69 (1990), [10.1201/9780429492860](#).
- [26] F. Takahashi, W. Yin and A.H. Guth, *QCD axion window and low-scale inflation*, *Phys. Rev. D* **98** (2018) 015042 [[1805.08763](#)].
- [27] P.W. Graham and A. Scherlis, *Stochastic axion scenario*, *Phys. Rev. D* **98** (2018) 035017 [[1805.07362](#)].
- [28] R.T. Co, L.J. Hall and K. Harigaya, *Axion Kinetic Misalignment Mechanism*, *Phys. Rev. Lett.* **124** (2020) 251802 [[1910.14152](#)].
- [29] C.-F. Chang and Y. Cui, *New Perspectives on Axion Misalignment Mechanism*, *Phys. Rev. D* **102** (2020) 015003 [[1911.11885](#)].
- [30] B. Barman, N. Bernal, N. Ramberg and L. Visinelli, *QCD Axion Kinetic Misalignment without Prejudice*, *Universe* **8** (2022) 634 [[2111.03677](#)].
- [31] P.J. Steinhardt and M.S. Turner, *Saving the Invisible Axion*, *Phys. Lett. B* **129** (1983) 51.
- [32] G. Lazarides, R.K. Schaefer, D. Seckel and Q. Shafi, *Dilution of Cosmological Axions by Entropy Production*, *Nucl. Phys. B* **346** (1990) 193.

- [33] M. Kawasaki, T. Moroi and T. Yanagida, *Can decaying particles raise the upper bound on the Peccei-Quinn scale?*, *Phys. Lett. B* **383** (1996) 313 [[hep-ph/9510461](#)].
- [34] G.F. Giudice, E.W. Kolb and A. Riotto, *Largest temperature of the radiation era and its cosmological implications*, *Phys. Rev. D* **64** (2001) 023508 [[hep-ph/0005123](#)].
- [35] D. Grin, T.L. Smith and M. Kamionkowski, *Axion constraints in non-standard thermal histories*, *Phys. Rev. D* **77** (2008) 085020 [[0711.1352](#)].
- [36] L. Visinelli and P. Gondolo, *Axion cold dark matter in non-standard cosmologies*, *Phys. Rev. D* **81** (2010) 063508 [[0912.0015](#)].
- [37] A.E. Nelson and H. Xiao, *Axion Cosmology with Early Matter Domination*, *Phys. Rev. D* **98** (2018) 063516 [[1807.07176](#)].
- [38] L. Visinelli and J. Redondo, *Axion Miniclusters in Modified Cosmological Histories*, *Phys. Rev. D* **101** (2020) 023008 [[1808.01879](#)].
- [39] N. Ramberg and L. Visinelli, *Probing the Early Universe with Axion Physics and Gravitational Waves*, *Phys. Rev. D* **99** (2019) 123513 [[1904.05707](#)].
- [40] N. Blinov, M.J. Dolan, P. Draper and J. Kozaczuk, *Dark matter targets for axionlike particle searches*, *Phys. Rev. D* **100** (2019) 015049 [[1905.06952](#)].
- [41] N. Blinov, M.J. Dolan and P. Draper, *Imprints of the Early Universe on Axion Dark Matter Substructure*, *Phys. Rev. D* **101** (2020) 035002 [[1911.07853](#)].
- [42] P. Arias, N. Bernal, D. Karamitros, C. Maldonado, L. Roszkowski and M. Venegas, *New opportunities for axion dark matter searches in nonstandard cosmological models*, *JCAP* **11** (2021) 003 [[2107.13588](#)].
- [43] P. Arias, N. Bernal, J.K. Osiński and L. Roszkowski, *Dark matter axions in the early universe with a period of increasing temperature*, *JCAP* **05** (2023) 028 [[2207.07677](#)].
- [44] M. Drees and F. Hajkarim, *Dark Matter Production in an Early Matter Dominated Era*, *JCAP* **02** (2018) 057 [[1711.05007](#)].
- [45] N. Bernal, M. Dutra, Y. Mambrini, K. Olive, M. Peloso and M. Pierre, *Spin-2 Portal Dark Matter*, *Phys. Rev. D* **97** (2018) 115020 [[1803.01866](#)].
- [46] D. Maity and P. Saha, *Connecting CMB anisotropy and cold dark matter phenomenology via reheating*, *Phys. Rev. D* **98** (2018) 103525 [[1801.03059](#)].
- [47] D. Maity and P. Saha, *CMB constraints on dark matter phenomenology via reheating in Minimal plateau inflation*, *Phys. Dark Univ.* **25** (2019) 100317 [[1804.10115](#)].
- [48] N. Bernal, F. Elahi, C. Maldonado and J. Unwin, *Ultraviolet Freeze-in and Non-Standard Cosmologies*, *JCAP* **11** (2019) 026 [[1909.07992](#)].
- [49] M.A.G. Garcia, K. Kaneta, Y. Mambrini and K.A. Olive, *Reheating and Post-inflationary Production of Dark Matter*, *Phys. Rev. D* **101** (2020) 123507 [[2004.08404](#)].
- [50] N. Bernal and Y. Xu, *Polynomial inflation and dark matter*, *Eur. Phys. J. C* **81** (2021) 877 [[2106.03950](#)].
- [51] L. Calibbi, F. D’Eramo, S. Junius, L. Lopez-Honorez and A. Mariotti, *Displaced new physics at colliders and the early universe before its first second*, *JHEP* **05** (2021) 234 [[2102.06221](#)].
- [52] A. Ahmed, B. Grzadkowski and A. Socha, *Higgs boson induced reheating and ultraviolet frozen-in dark matter*, *JHEP* **02** (2023) 196 [[2207.11218](#)].

- [53] B. Barman, N. Bernal, Y. Xu and O. Zapata, *Ultraviolet freeze-in with a time-dependent inflaton decay*, *JCAP* **07** (2022) 019 [2202.12906].
- [54] A. Banerjee and D. Chowdhury, *Fingerprints of freeze-in dark matter in an early matter-dominated era*, *SciPost Phys.* **13** (2022) 022 [2204.03670].
- [55] N. Bernal and Y. Xu, *WIMPs during reheating*, *JCAP* **12** (2022) 017 [2209.07546].
- [56] P.N. Bhattiprolu, G. Elor, R. McGehee and A. Pierce, *Freezing-in hadrophilic dark matter at low reheating temperatures*, *JHEP* **01** (2023) 128 [2210.15653].
- [57] M.R. Haque, D. Maity and R. Mondal, *WIMPs, FIMPs, and Inflaton phenomenology via reheating*, *CMB and  $\Delta N_{eff}$* , **2301.01641**.
- [58] D. Chowdhury and A. Hait, *Thermalization in the presence of a time-dependent dissipation and its impact on dark matter production*, **2302.06654**.
- [59] J. Silva-Malpartida, N. Bernal, J. Jones-Pérez and R.A. Lineros, *From WIMPs to FIMPs with Low Reheating Temperatures*, **2306.14943**.
- [60] M. Becker, E. Copello, J. Harz, J. Lang and Y. Xu, *Confronting Dark Matter Freeze-In during Reheating with Constraints from Inflation*, **2306.17238**.
- [61] X. Gan and Y.-D. Tsai, *Cosmic Millicharge Background and Reheating Probes*, **2308.07951**.
- [62] I.G. Irastorza and J. Redondo, *New experimental approaches in the search for axion-like particles*, *Prog. Part. Nucl. Phys.* **102** (2018) 89 [1801.08127].
- [63] C.B. Adams et al., *Axion Dark Matter*, in *Snowmass 2021*, 3, 2022 [2203.14923].
- [64] M.A.G. Garcia, K. Kaneta, Y. Mambrini and K.A. Olive, *Inflaton Oscillations and Post-Inflationary Reheating*, *JCAP* **04** (2021) 012 [2012.10756].
- [65] M.S. Turner, *Coherent Scalar Field Oscillations in an Expanding Universe*, *Phys. Rev. D* **28** (1983) 1243.
- [66] R. Allahverdi, R. Brandenberger, F.-Y. Cyr-Racine and A. Mazumdar, *Reheating in Inflationary Cosmology: Theory and Applications*, *Ann. Rev. Nucl. Part. Sci.* **60** (2010) 27 [1001.2600].
- [67] M.A. Amin, M.P. Hertzberg, D.I. Kaiser and J. Karouby, *Nonperturbative Dynamics Of Reheating After Inflation: A Review*, *Int. J. Mod. Phys. D* **24** (2014) 1530003 [1410.3808].
- [68] K.D. Lozanov, *Lectures on Reheating after Inflation*, **1907.04402**.
- [69] R. Kallosh and A. Linde, *Universality Class in Conformal Inflation*, *JCAP* **07** (2013) 002 [1306.5220].
- [70] A.A. Starobinsky, *A New Type of Isotropic Cosmological Models Without Singularity*, *Phys. Lett. B* **91** (1980) 99.
- [71] M. Drees and Y. Xu, *Small field polynomial inflation: reheating, radiative stability and lower bound*, *JCAP* **09** (2021) 012 [2104.03977].
- [72] M. Drees and Y. Xu, *Large field polynomial inflation: parameter space, predictions and (double) eternal nature*, *JCAP* **12** (2022) 005 [2209.07545].
- [73] Y. Xu, *Polynomial Inflation and Its Aftermath*, Ph.D. thesis, U. Bonn (main), 2022.
- [74] K. Ichikawa, T. Suyama, T. Takahashi and M. Yamaguchi, *Primordial Curvature*

- Fluctuation and Its Non-Gaussianity in Models with Modulated Reheating*, *Phys. Rev. D* **78** (2008) 063545 [0807.3988].
- [75] K.D. Lozanov and M.A. Amin, *Equation of State and Duration to Radiation Domination after Inflation*, *Phys. Rev. Lett.* **119** (2017) 061301 [1608.01213].
- [76] M.R. Haque and D. Maity, *Gravitational reheating*, *Phys. Rev. D* **107** (2023) 043531 [2201.02348].
- [77] J.F. Dufaux, G.N. Felder, L. Kofman, M. Peloso and D. Podolsky, *Preheating with trilinear interactions: Tachyonic resonance*, *JCAP* **07** (2006) 006 [hep-ph/0602144].
- [78] D. Maity and P. Saha, *(P)reheating after minimal Plateau Inflation and constraints from CMB*, *JCAP* **07** (2019) 018 [1811.11173].
- [79] P. Saha, S. Anand and L. Sriramkumar, *Accounting for the time evolution of the equation of state parameter during reheating*, *Phys. Rev. D* **102** (2020) 103511 [2005.01874].
- [80] M. Peloso and L. Sorbo, *Preheating of massive fermions after inflation: Analytical results*, *JHEP* **05** (2000) 016 [hep-ph/0003045].
- [81] R.T. Co, Y. Mambrini and K.A. Olive, *Inflationary gravitational leptogenesis*, *Phys. Rev. D* **106** (2022) 075006 [2205.01689].
- [82] B. Barman, S. Cléry, R.T. Co, Y. Mambrini and K.A. Olive, *Gravity as a portal to reheating, leptogenesis and dark matter*, *JHEP* **12** (2022) 072 [2210.05716].
- [83] G. Grilli di Cortona, E. Hardy, J. Pardo Vega and G. Villadoro, *The QCD axion, precisely*, *JHEP* **01** (2016) 034 [1511.02867].
- [84] S. Borsanyi et al., *Calculation of the axion mass based on high-temperature lattice quantum chromodynamics*, *Nature* **539** (2016) 69 [1606.07494].
- [85] PARTICLE DATA GROUP collaboration, *Review of Particle Physics*, *PTEP* **2022** (2022) 083C01.
- [86] M. Kawasaki, K. Kohri and N. Sugiyama, *MeV scale reheating temperature and thermalization of neutrino background*, *Phys. Rev. D* **62** (2000) 023506 [astro-ph/0002127].
- [87] S. Hannestad, *What is the lowest possible reheating temperature?*, *Phys. Rev. D* **70** (2004) 043506 [astro-ph/0403291].
- [88] P.W. Graham, I.G. Irastorza, S.K. Lamoreaux, A. Lindner and K.A. van Bibber, *Experimental Searches for the Axion and Axion-Like Particles*, *Ann. Rev. Nucl. Part. Sci.* **65** (2015) 485 [1602.00039].
- [89] ADMX collaboration, *A Search for Invisible Axion Dark Matter with the Axion Dark Matter Experiment*, *Phys. Rev. Lett.* **120** (2018) 151301 [1804.05750].
- [90] ADMX collaboration, *Extended Search for the Invisible Axion with the Axion Dark Matter Experiment*, *Phys. Rev. Lett.* **124** (2020) 101303 [1910.08638].
- [91] N. Crisosto, P. Sikivie, N.S. Sullivan, D.B. Tanner, J. Yang and G. Rybka, *ADMX SLIC: Results from a Superconducting LC Circuit Investigating Cold Axions*, *Phys. Rev. Lett.* **124** (2020) 241101 [1911.05772].
- [92] ADMX collaboration, *Search for Invisible Axion Dark Matter in the 3.3–4.2  $\mu\text{eV}$  Mass Range*, *Phys. Rev. Lett.* **127** (2021) 261803 [2110.06096].

- [93] ADMX collaboration, *Dark matter axion search using a Josephson Traveling wave parametric amplifier*, *Rev. Sci. Instrum.* **94** (2023) 044703 [2110.10262].
- [94] S. Lee, S. Ahn, J. Choi, B.R. Ko and Y.K. Semertzidis, *Axion Dark Matter Search around  $6.7 \mu\text{eV}$* , *Phys. Rev. Lett.* **124** (2020) 101802 [2001.05102].
- [95] J. Jeong, S. Youn, S. Bae, J. Kim, T. Seong, J.E. Kim et al., *Search for Invisible Axion Dark Matter with a Multiple-Cell Haloscope*, *Phys. Rev. Lett.* **125** (2020) 221302 [2008.10141].
- [96] CAPP collaboration, *First Results from an Axion Haloscope at CAPP around  $10.7 \mu\text{eV}$* , *Phys. Rev. Lett.* **126** (2021) 191802 [2012.10764].
- [97] Y. Lee, B. Yang, H. Yoon, M. Ahn, H. Park, B. Min et al., *Searching for Invisible Axion Dark Matter with an 18 T Magnet Haloscope*, *Phys. Rev. Lett.* **128** (2022) 241805 [2206.08845].
- [98] J. Kim et al., *Near-Quantum-Noise Axion Dark Matter Search at CAPP around  $9.5 \mu\text{eV}$* , *Phys. Rev. Lett.* **130** (2023) 091602 [2207.13597].
- [99] E. Todarello, M. Regis, J. Reynoso-Cordova, M. Taoso, D. Vaz, J. Brinchmann et al., *Robust bounds on ALP dark matter from dwarf spheroidal galaxies in the optical MUSE-Faint survey*, **2307.07403**.
- [100] DMRADIO collaboration, *Projected sensitivity of DMRadio-m3: A search for the QCD axion below  $1 \mu\text{eV}$* , *Phys. Rev. D* **106** (2022) 103008 [2204.13781].
- [101] D. Alesini et al., *KLASH Conceptual Design Report*, **1911.02427**.
- [102] A. Díaz-Morcillo et al., *Design of New Resonant Haloscopes in the Search for the Dark Matter Axion: A Review of the First Steps in the RADES Collaboration*, *Universe* **8** (2021) 5 [2111.14510].
- [103] I. Stern, *ADMX Status*, *PoS ICHEP2016* (2016) 198 [1612.08296].
- [104] J. De Miguel and J.F. Hernández-Cabrera, *Discovery prospects with the Dark-photons  $\mathcal{E}$  Axion-Like particles Interferometer—part I*, **2303.03997**.
- [105] M. Lawson, A.J. Millar, M. Pancaldi, E. Vitagliano and F. Wilczek, *Tunable axion plasma haloscopes*, *Phys. Rev. Lett.* **123** (2019) 141802 [1904.11872].
- [106] S. Beurthey et al., *MADMAX Status Report*, **2003.10894**.
- [107] B.T. McAllister, G. Flower, J. Kruger, E.N. Ivanov, M. Goryachev, J. Bourhill et al., *The ORGAN Experiment: An axion haloscope above 15 GHz*, *Phys. Dark Univ.* **18** (2017) 67 [1706.00209].
- [108] B. Aja et al., *The Canfranc Axion Detection Experiment (CADEx): search for axions at 90 GHz with Kinetic Inductance Detectors*, *JCAP* **11** (2022) 044 [2206.02980].
- [109] BREAD collaboration, *Broadband Solenoidal Haloscope for Terahertz Axion Detection*, *Phys. Rev. Lett.* **128** (2022) 131801 [2111.12103].
- [110] M. Baryakhtar, J. Huang and R. Lasenby, *Axion and hidden photon dark matter detection with multilayer optical haloscopes*, *Phys. Rev. D* **98** (2018) 035006 [1803.11455].
- [111] C. O’Hare, “cajohare/axionlimits: Axionlimits.” <https://cajohare.github.io/AxionLimits/>, July, 2020. 10.5281/zenodo.3932430.